

Solution Structure of the DFF-C Domain of DFF45/ICAD. A Structural Basis for the Regulation of Apoptotic DNA Fragmentation

Kay Fukushima, Jun Kikuchi, Seizo Koshiba, Takanori Kigawa
Yutaka Kuroda* and Shigeyuki Yokoyama

Protein Research Group
Genomic Sciences Center
RIKEN Yokohama Institute
1-7-22, Suehiro-cho
Tsurumi, Yokohama
Kanagawa 230-0045, Japan

DFF45/ICAD has dual functions in the final stage of apoptosis, by acting as both a folding chaperone and a DNase inhibitor of DFF40/CAD. Here, we present the solution structure of the C-terminal domain of DFF45, which is essential for its chaperone-like activity. The structure of this domain (DFF-C) consists of four α helices, which are folded in a novel helix-packing arrangement. The 3D structure reveals a large cluster of negatively charged residues on the molecular surface of DFF-C. This observation suggests that charge complementation plays an important role in the interaction of DFF-C with the positively charged catalytic domain of DFF40, and thus for the chaperone activity of DFF45. The structure of DFF-C also provides a rationale for the loss of the chaperone activity in DFF35, a short isoform of DFF45. Indeed, in DFF35, the amino acid sequence is truncated in the middle of the second α helix constituting the structure of DFF-C, and thus both the hydrophobic core and the cluster of negative charges are disrupted.

© 2002 Elsevier Science Ltd. All rights reserved

Keywords: NMR; chaperone-like activity; stable domain; apoptosis; DREP-1

*Corresponding author

Introduction

Apoptosis is a programmed cell death process that controls cell number and proliferation during animal development.¹ Among its distinctive features, the degradation of chromosomal DNA into nucleosomal fragments is considered to be a morphological hallmark of apoptosis.^{2,3} DNA fragmentation in apoptosis is caused by DFF40 (DNA fragmentation factor 40k)/CAD (caspase-activated deoxyribonuclease), which is activated through the caspase cascade pathway.

In non-apoptotic cells, DFF40 is complexed with its inhibitor, DFF45 (ICAD).^{4–6} The activation of

the DFF40/DFF45 complex occurs through the caspase 3-mediated cleavage of DFF45 at residues 117 and 224, which results in three DFF45 fragments that are then released from DFF40.^{4,6} In addition to its DNase inhibitory activity, DFF45 acts as a DFF40-specific folding chaperone. This chaperone activity is demonstrated by the absence of DNA fragmentation or chromatin condensation in mice expressing DFF40 but lacking DFF45.⁷ This observation indicates that DFF45 is required absolutely for the production of functional DFF40.^{7,8} Both the DNase inhibitory and the chaperone-like activities of DFF45 seem to be essential for the strict regulation of DNA fragmentation in apoptosis.⁸

Human DFF45 (hICAD) consists of 331 residues and appears to be a multi-functional/multi-domain protein, with an N-terminal domain (CD⁹ or NTD¹⁰) constituting a regulatory domain. Besides being present in DFF40 and DFF45,¹¹ the CD domain is found in several other caspase-associated proteins, such as CIDE,¹² and DREP-1,^{12,13} the *Drosophila* homologue of DFF45. In DFF45, the CD domain corresponds to the N-terminal fragment produced by caspase cleavage, and

Abbreviations used: NOE, nuclear overhauser enhancement; hNOE, heteronuclear NOE; DFF40, DNA fragmentation factor 40k; CAD, caspase-activated deoxyribonuclease; DFF45 (ICAD), inhibitor of DFF40; hICAD, human ICAD; mICAD, mouse ICAD; DFF-C, DFF-chaperone domain; HSQC, heteronuclear single-quantum coherence; IPAP-HSQC, in-phase anti-phase HSQC; TAD, torsion angle space dynamics.

E-mail address of the corresponding author: kuroda@gsc.riken.go.jp

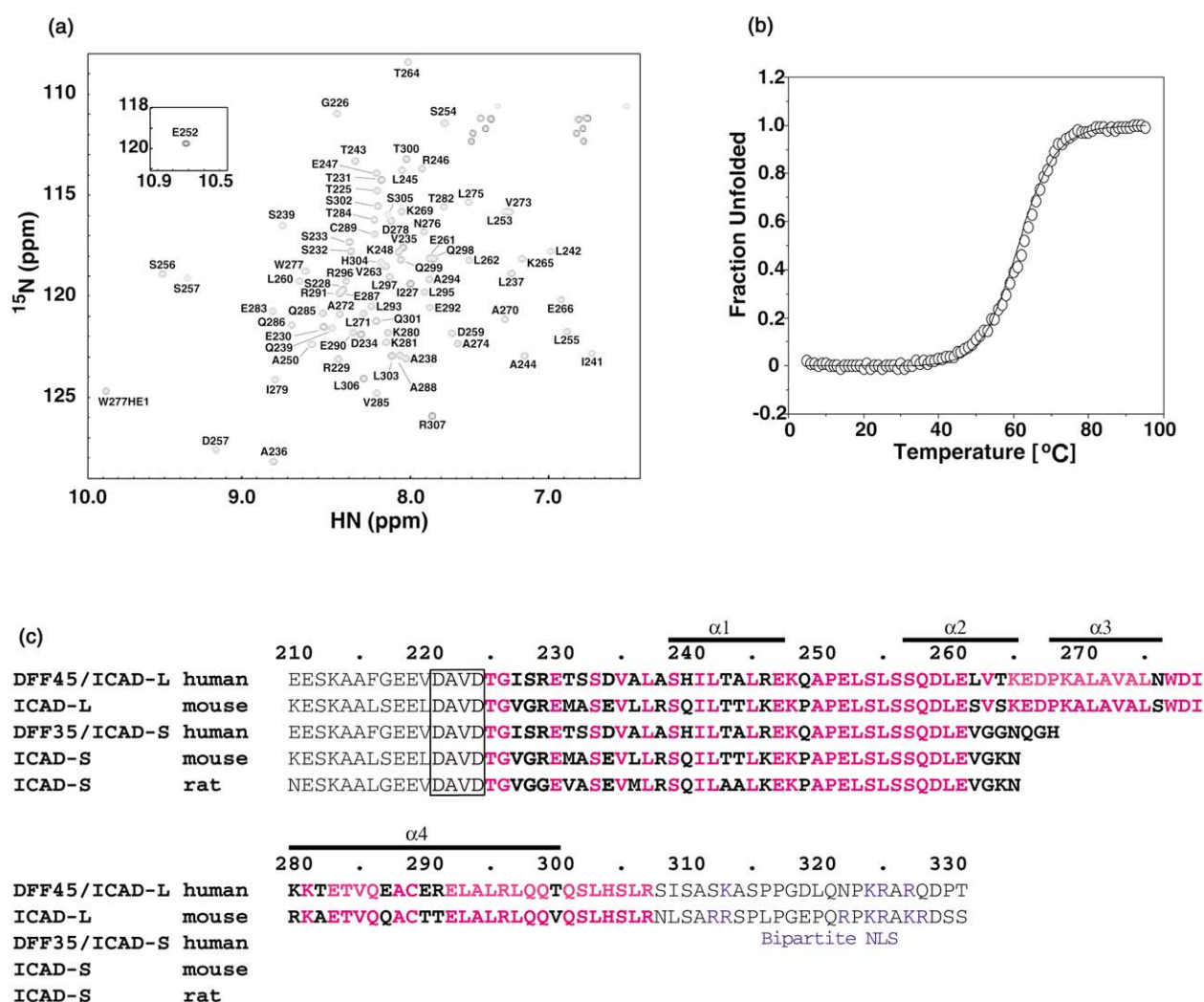


Figure 1. (a) HSQC spectrum of DFF-C at pH 6.5 and 25 °C. The peaks are labeled according to their amino acid types and residue numbers. The low-field shifted E252 signal is shown in the inset. (b) Thermal denaturation curve of DFF-C at pH 6.5. Open circles represent the experimental CD data at 222 nm. The calculated curve for a two-state model with a melting temperature of 61 °C and a van't Hoff enthalpy of 189 kJ/mol is represented by a black line. (c) Sequence alignment of hDFF45 with mICAD (mouse DFF45), DFF35 (short isoform of hDFF45), mICAD-S (short isoform of mICAD), and rICAD-S. The α helices, identified in the averaged NMR structure by DSSP,³⁵ are represented by lines above the hDFF45 sequence. Residues recognized by caspase 3 are boxed, and those forming the DFF-C domain are shown with bold characters. Conserved residues are red, while residues not conserved in the mouse sequence are black. The DFF-C sequence that we analyzed starts at T225 and ends at R307. Our construct has four additional residues (GSHM) at the N terminus, due to the thrombin cleavage site in the pET15b construct.

it mediates the intermolecular interactions responsible for the inhibition of DFF40 by DFF45, by interacting with the CD domain of DFF40.⁹

So far, the C-terminal region of DFF45 (residues 118–331) has been found only in the human and in the mouse DFF45 (usually referred as ICAD or mICAD). Yet, this region plays an essential role in the inhibition of DFF40 by binding to its C-terminal catalytic domain.¹⁴ Recent reports have shown that DFF35/ICAD-S, a short isoform of DFF45/ICAD that ends at residue 268 and lacks the 63 C-terminal residues of DFF45, can inhibit the DNase activity of DFF40/CAD, both *in vitro*¹⁵ and *in vivo*.¹⁶

In addition to blocking the DNase activity of DFF40, the C-terminal region of DFF45 is impor-

tant for the DFF40-specific folding chaperone activity.^{4,8,17} Especially, residues 262–331 of DFF45 have a critical role in the chaperone activity, as demonstrated by the ability of DFF45 to refold DFF40, whereas no such folding chaperone activity is observed for DFF35.^{15,17}

Here, we have investigated the structure of the C-terminal region of DFF45, which is essential for the DFF40-specific chaperone activity. Specifically, we show that an 83 residue domain located at the C-terminal end of DFF45 (residues 225–307), which includes the 37 C-terminal residues of DFF35, forms a stable structural domain. The solution structure of this domain (DFF-C, for DFF chaperone domain) indicates that DFF-C cannot

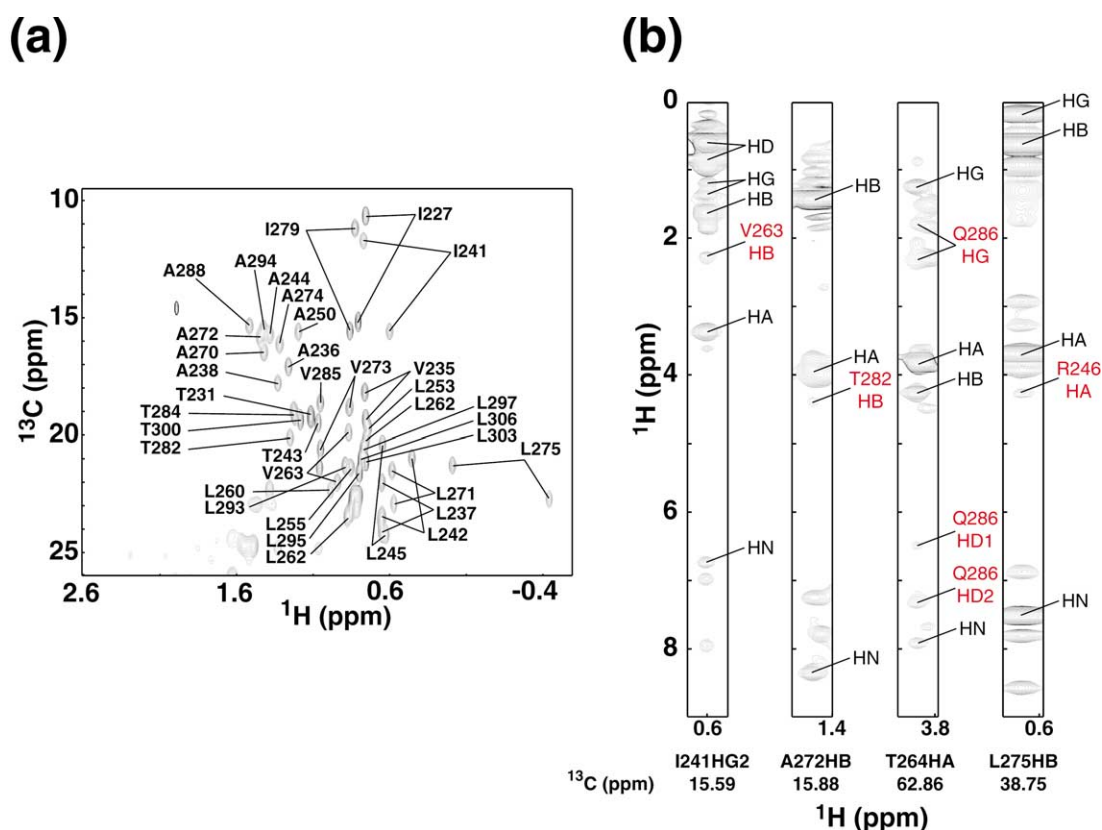


Figure 2. (a) Expanded view of the methyl regions of the ^1H - ^{13}C HSQC spectrum of DFF-C at pH 6.5 and 25 °C. The signals are labeled according to their amino acid types and residue numbers. (b) Selected slices of the 3D ^1H - ^{13}C NOEY-HSQC spectrum of DFF-C. The inter-helix NOEs, which were useful to determine the global fold of DFF-C, are shown in red.

fold properly in DFF35, because the amino acid sequence ends at residue 261, i.e. in the middle of the DFF-C domain. Furthermore, the presence of a large cluster of negative charges on the molecular surface of DFF-C suggests that charge complementation is important in the chaperone activity of DFF45. Additionally, the structure of DFF-C, combined with analyses of the sequences of DFF45 and its *Drosophila* homologue, DREP-1, suggests that DREP-1^{12,13} lacks a DFF-C domain.

Results and Discussion

DFF-C is a stable domain that can fold in isolation

On the basis of previous biochemical reports indicating that DFF45, but not DFF35, exhibits a chaperone activity,^{15,17} we hypothesized the presence of an independently folded C-terminal domain in DFF45. The precise boundaries of this domain were determined by N-terminal sequencing and matrix-assisted laser desorption/ionisation time-of-flight (MALDI-TOF) mass spectroscopy of a fragment stable to digestion by trypsin. The strong resistance to proteolytic degradation (two hours at room-temperature at pH 7.5,

with a protein concentration of 500 $\mu\text{g}/\text{ml}$ and a trypsin concentration of 0.5 $\mu\text{g}/\text{ml}$) is by itself an indication of a stable structural domain that can fold in isolation. The structural domain we identified, DFF-C, begins just after the caspase 3 cleavage site and ends at the start of a nuclear-localization signal peptide.¹⁸ The sharp and dispersed peaks in the ^1H - ^{15}N heteronuclear single-quantum coherence (HSQC) spectrum (Figure 1(a)) indicate a well-folded structure. All of the peaks corresponding to residues 225–307 are visible in the HSQC spectra, and the well-folded structure is further substantiated by the reversible thermal denaturation curve with a midpoint temperature of 61 °C (Figure 1(b)). The resulting van't Hoff enthalpy ($\Delta H = 189$ kJ/mol) agrees well with values typically observed upon the unfolding of globular proteins of this size.

Although a full picture of the chaperone activity will require an understanding of the synergistic binding of the multiple DFF45 domains to DFF40,¹⁴ the presence of a stable structural domain at the C-terminal end of DFF45 provides further evidence for the modular nature of DFF45. In particular, this finding corroborates a model in which DFF45, or at least the DFF-C domain, is first natively folded and then binds to the nascent DFF40 to act as a folding chaperone.^{4,7,8}

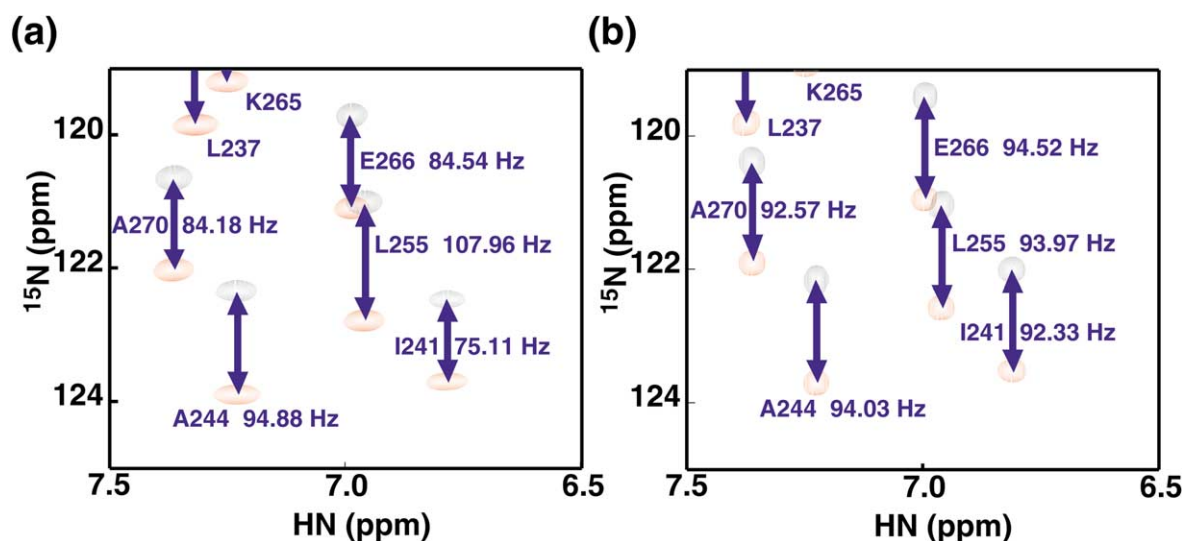


Figure 3. Measurement of the $1J_{\text{NH}}$ values. IPAP ^1H - ^{15}N HSQC (a) in the presence and (b) in the absence of 20 mg/ml of Pf1 phage. (a) The lines-shape in the f_2 direction is relatively wide because of the long-range ^1H - ^1H residual dipolar couplings originating from the (un-deuterated) side-chain protons. The small difference in the ^1H chemical shift value of L237 might indicate the existence of non-specific binding. However, L237 is located at the unstructured N-terminal end of DFF-C domain, and the other ^1H chemical shift values remain unchanged. Notice also that the ^{15}N chemical shift values are unchanged between the two spectra, the shifts in the ^{15}N direction are due to the residual dipolar coupling and the residual chemical shift anisotropy.

NMR structure determination

We carried out the NMR experiments at pH 6.5, where DFF-C was highly soluble and the amide proton exchange rates were relatively low. At a lower pH, DFF-C had a tendency to aggregate, especially when the pH was close to its isoelectric point of 5.1. The sequential assignment could be achieved using standard (^{15}N and ^{13}C) heteronuclear experiments (also see Materials and Methods). The secondary structures of DFF-C, as determined by TALOS and the characteristic NOE patterns,¹⁹ are composed of four helices, located at residues 239–247 ($\alpha 1$), 257–265 ($\alpha 2$), 268–275 ($\alpha 3$), and 280–300 ($\alpha 4$) (Figure 1(c)). The sharp and well-dispersed peaks in the ^1H - ^{13}C HSQC spectra (Figure 2(a)) were helpful for obtaining the almost complete assignment of the side-chain atoms, including the methyl groups. A careful assignment of the inter-side-chain NOEs between the helices (Figure 2(b)) was essential to determine the initial global fold of DFF-C. Especially, several inter-side-chain NOEs between residues contributing to the hydrophobic core around W277 facilitated the determination of the relative orientations of $\alpha 2$, $\alpha 3$ and $\alpha 4$. On the other hand, $\alpha 1$ interacts with the other helices mainly through its C-terminal end, and most long-range NOE involving $\alpha 1$ are located at its C-terminal end (12 and seven long-range NOE from L245 and R246, respectively). As a result, the position of the N-terminal end of $\alpha 1$ relies on one long-range NOE from S239 and five long-range NOEs from I241 and L242, and the orientation of $\alpha 1$ relative to the other helices was relatively laborious to specify.

The structure of DFF-C was calculated on the basis of 841 NOE-derived distance constraints. In addition to these NOE constraints, we refined the solution structure of DFF-C by introducing restraints derived from the residual dipolar coupling values. Considering that DFF-C is negatively charged, we chose Pf1 phage as the nematogen for the residual dipolar coupling measurements.²⁰ The peaks in the IPAP-HSQC spectra were well dispersed and resolved in both the isotropic and the aligned states, and we were able to determine 49 coupling values (Figure 3). The introduction of restraints derived from the residual dipolar coupling values improved the precision (RMSD from the average structure) of the calculated structure by more than 0.2 Å (Table 1; Figure 4(a)). Figure 4(b) shows how the inertia tensor of the DFF-C lies with respect to the alignment tensor determined for the Pf1 phage media. The long axis for these two tensors differed by approximately $2\pi/15$ rad (24.5°) because of the weak electrostatic interactions between the phage and the DFF-C.

Description of the structure

The structure of DFF-C is formed by four helices, with $\alpha 2$ and $\alpha 3$ packing against a long C-terminal helix ($\alpha 4$) (Figure 4). The side-chains of P251 and W277, which are located, respectively, in the loops between $\alpha 1$ and $\alpha 2$ and between $\alpha 3$ and $\alpha 4$, are inserted into the hydrophobic core and help to stabilize the structure of DFF-C. On the other hand, the first helix ($\alpha 1$) protrudes almost perpendicularly from the structure constituted by $\alpha 2$, $\alpha 3$,

Table 1. Structural statistics for the ten best NMR-derived DFF-C structures

NOE distance restraints	
All ^a	841
Intraresidue ($ i - j = 0$)	355
Sequential ($ i - j = 1$)	214
Medium-range ($2 \leq i - j \leq 4$)	191
$i, i + 2$	73
$i, i + 3$	80
$i, i + 4$	38
Long-range ($ i - j \geq 5$)	84
Dihedral angle	168
Hydrogen bonds ^b	46
Dipolar coupling ^b	49
Average RMSD to the mean structure	
Backbone (residues 239–295)	$0.63 \text{ \AA} \pm 0.27 \text{ \AA}$
Heavy atoms (residues 239–295)	$1.03 \text{ \AA} \pm 0.26 \text{ \AA}$
Backbone (residues 239–295) without residual dipolar	$0.85 \text{ \AA} \pm 0.22 \text{ \AA}$
Heavy atoms (residues 239–295) without residual dipolar	$1.49 \text{ \AA} \pm 0.27 \text{ \AA}$
Backbone (helical region) ^c	$0.58 \text{ \AA} \pm 0.28 \text{ \AA}$
Heavy atoms (helical region) ^c	$1.14 \text{ \AA} \pm 0.15 \text{ \AA}$
RMSD from experimental restraints	
NOE	0.0027 \AA
Dihedral angle	0.060 deg.
Residual dipolar coupling	0.0547 Hz
Ramachandran plot ^d	
Residues in most favored regions (%)	47 (81.0)
Residues in additionally allowed regions (%)	10 (17.2)
Residues in generously allowed regions (%)	1 (1.7)
Residues in disallowed regions (%)	0 (0)

^a No violation of the NOE-derived constraints larger than 0.4 \AA is observed in any of the ten structures.

^b Hydrogen bonds and dipolar coupling were introduced at the second stage of calculations.

^c Residues included in the calculation are: 239–247, 257–265, 268–275, and 280–295.

^d Calculated for the averaged structure using PROCHECK.³⁸

and $\alpha 4$. An extensive network of hydrophobic interactions stabilizes this helical structure (Figures 4 and 6(b)). The center of the hydrophobic core is formed by L242 and L245 on $\alpha 1$, L260 and V263 on $\alpha 2$, L271, and L275 on $\alpha 3$, and V285, Q286, C289, and L293 on $\alpha 4$. Two hydrophobic residues at the C-terminal end of $\alpha 4$, L295 and L297, are located at the periphery of the hydrophobic core. Additionally, three hydrophobic residues (L262, V273, and I279) located on the helices (or just before the start of a helix) are exposed on the protein surface (average accessibility over 60%). However, these residues are isolated from each other, and do not form a large hydrophobic patch (Figure 6(b)).

Despite the relatively simple structure composed of only four helices, a DALI search^{21†} against 3156 sequence families representing 30,071 protein structures showed that this arrangement of helices is novel by its distinct helix-packing mode (Figure 4; no structure with a Z-score > 3.6 was found). Low structural similarities with helical bundle structures were reported. Among the structures with a DALI score over 2.0 (which is an usual threshold value for significance), a fragment corresponding to residues 422–481 of carbomoyl phosphate synthetase was the only one containing four

helices, and the other contained only three helices. Even in this case, the detailed helix packing arrangement differed from that of DFF-C.

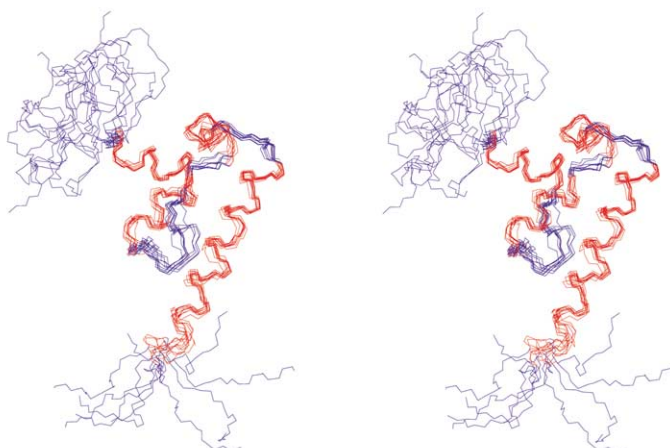
Dynamic features of DFF-C

The central structure formed by the four helices of DFF-C was essentially rigid on both the fast (pico- to nanosecond) and slow ($>$ millisecond) time-scales, as revealed by the T_2 and the ^1H – ^{15}N heteronuclear NOEs (hNOE) experiments, and the H^2H -exchange experiment, respectively (Figure 5). The order of magnitude of the T_2 values in the DFF-C core region was 100 ms, which is reasonable for a protein of this size. Consistent with the fast motions suggested by the T_2 and hNOE experiments (Figure 5), neither the 15 N-terminal nor the seven C-terminal residues have a defined structure in DFF-C (Figure 4(a)). However, some structures might form in the intact DFF45 or in the DFF40/DFF45 complex.

On the slow time-scale, the exchange rates of the L253 and L255 amide protons, which are located in the long 248–256 loop, are slow. Indeed, the protection factors²² of L253 and L255 are similar to those of residues belonging to loop 266–267 and loop 276–279, which are only two and four residues long, respectively. In addition, we observed several long-range NOEs assigned to residues in this long loop (Figure 5), and residues 249–253

† www2.ebi.ac.uk DALI server

(a)



(b)

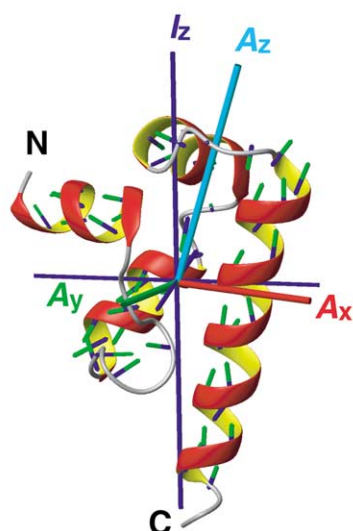


Figure 4. (a) Stereo view of ten superimposed NMR-derived structures with the lowest overall energy and without NOE restraint violations >0.4 Å. The α -helices are shown in red. (b) Ribbon model of DFF-C with the axis of the overall alignment tensor in the anisotropic medium (A_x , A_y , A_z) and of the inertial tensor (I_x , I_y , I_z). The amide hydrogen and nitrogen atoms of 49 residues whose residual dipolar coupling values were used in the structure calculation, are shown in green and blue, respectively. Residual dipolar coupling constraints were used for residues with ^1H - ^{15}N heteronuclear NOE larger than 0.6. The alignment tensor was calculated with the program SSIA,³⁶ using the lowest-energy structure. The long axis of the alignment tensor (A_z) differs by approximately $2\pi/15$ from the inertia tensor (I_z).

and L255 were buried in the final structure. Together with the results of the H^2H -exchange experiments, these observations suggest that, in spite of its extended conformation, this loop participates actively in the structure of DFF-C.

A large cluster of negatively charged residues

The DFF-C domain contains almost as many positive as negative charges, with 12 positive (R, K, H) and 13 negative (D, E) residues and a calculated isoelectric point of 5.11 (Figure 1). However, while the positive residues are distributed rather evenly on the molecular surface of DFF-C, the negative residues are located close to each other (Figure 6(a)). A surface representation of the DFF-C electrostatic potential indeed reveals a large negative surface formed by E283, E287, and E290 on $\alpha 4$ and extended by D259, E261, D267, and E266 (Figure 6(a)). With the exception of E287Q and E290T, all of the residues contributing to the negative surface are conserved in the mouse DFF45 sequence (mICAD; Figure 1(c)). Thus, we hypothesize that this large cluster of negative residues mediates the interaction of DFF-C with the

positively charged C-terminal domain of DFF40, which has a calculated isoelectric point of 9.8 and bears the nuclease activity of DFF40.¹¹

The structure of DFF-C suggests a straightforward explanation for the lack of chaperone activity in DFF35:^{15,17} The sequence of DFF35 ends at residue 261, in the middle of the second helix $\alpha 2$ (Figure 6(c)). With the sequence ending at residue 261, the hydrophobic core of DFF-C is disrupted, which would prevent this domain from folding correctly (Figure 1(c)). As a result, the large negative surface is not present in DFF35.

Along with the disruption of the negative residue cluster, another putative cause for the lack of the chaperone activity in DFF35 is the loss of the cysteine residues in DFF35. Indeed, the chaperone activity of DFF45 is observed, *in vitro*, under highly reducing conditions,⁸ and thus cysteine residues might be involved in the chaperone activity of DFF-C. Among the many cysteine residues within the DFF40/DFF45 complex, C289 is the only one that is present in DFF45 but not in DFF35. However, this C289 residue is embedded in the center of the negative surface (Figure 6(b)), and is buried completely within the hydrophobic core.

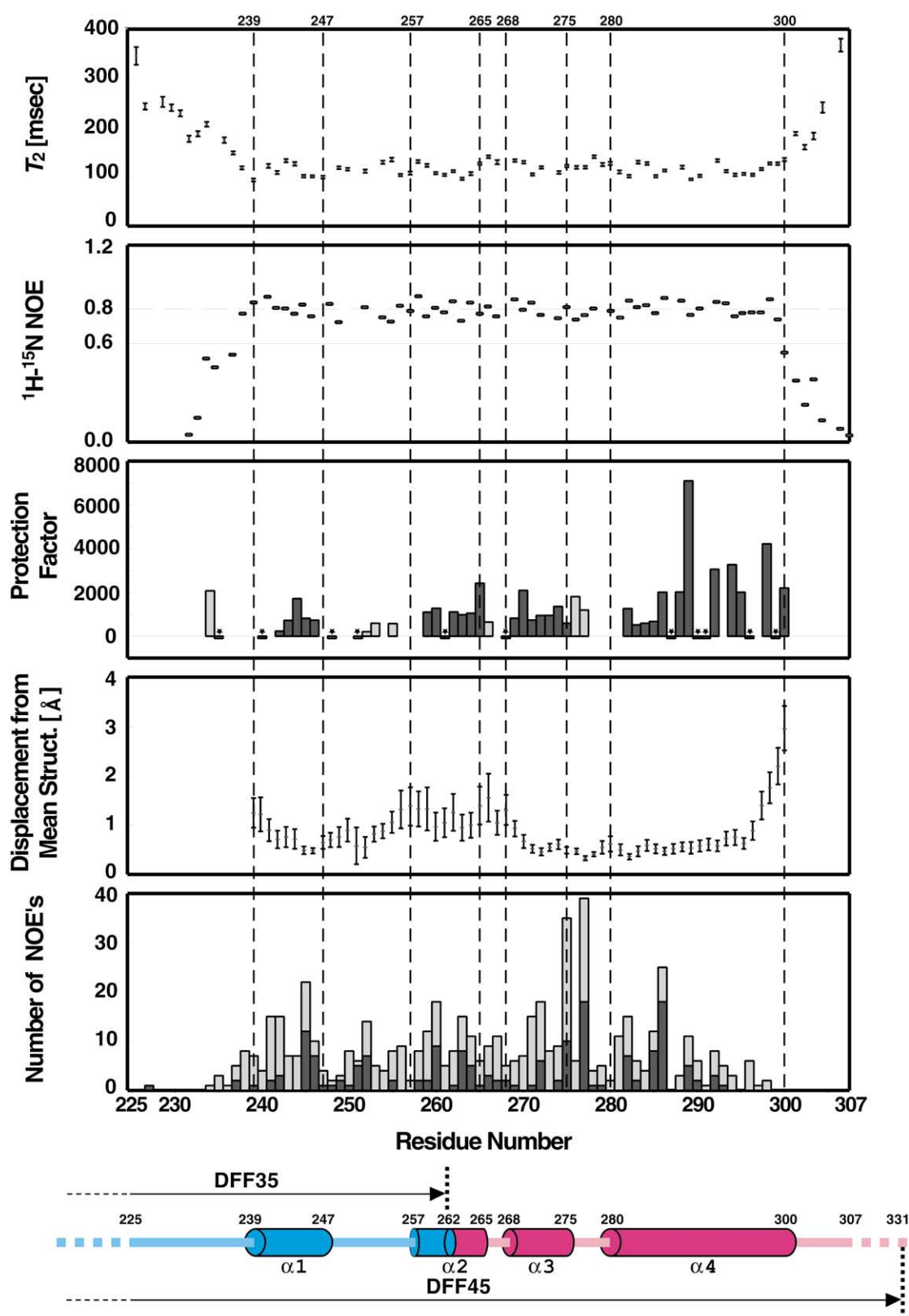


Figure 5. Protein dynamics and structural properties of DFF-C. The T_2 values, the heteronuclear NOEs, protection factors, the residue's averaged displacement, and the number of middle-range (open bars) and long-range NOEs (filled bars) observed for each residue are plotted *versus* the residue number. The continuous horizontal line at 0.6 in the heteronuclear NOE plot represents the standard criteria for a rigid structure. The broken line at 0.8 represents the average heteronuclear NOE value for residues 239–300. The heteronuclear NOE values for residues in α helices varied from 0.794 to 0.819. The heteronuclear NOE values were slightly smaller for residues in loop regions (0.774–0.793). Residues for which protection factors could not be determined because of peak overlap are indicated by stars and are distinguished from those with small values. The residue's average displacement is calculated for the ten best NMR structures, and the error bars show the standard deviations. At the bottom of the panel, the diagram indicates the locations of the α helices, and the extent of DFF35 and DFF45, by cyan and magenta, respectively.

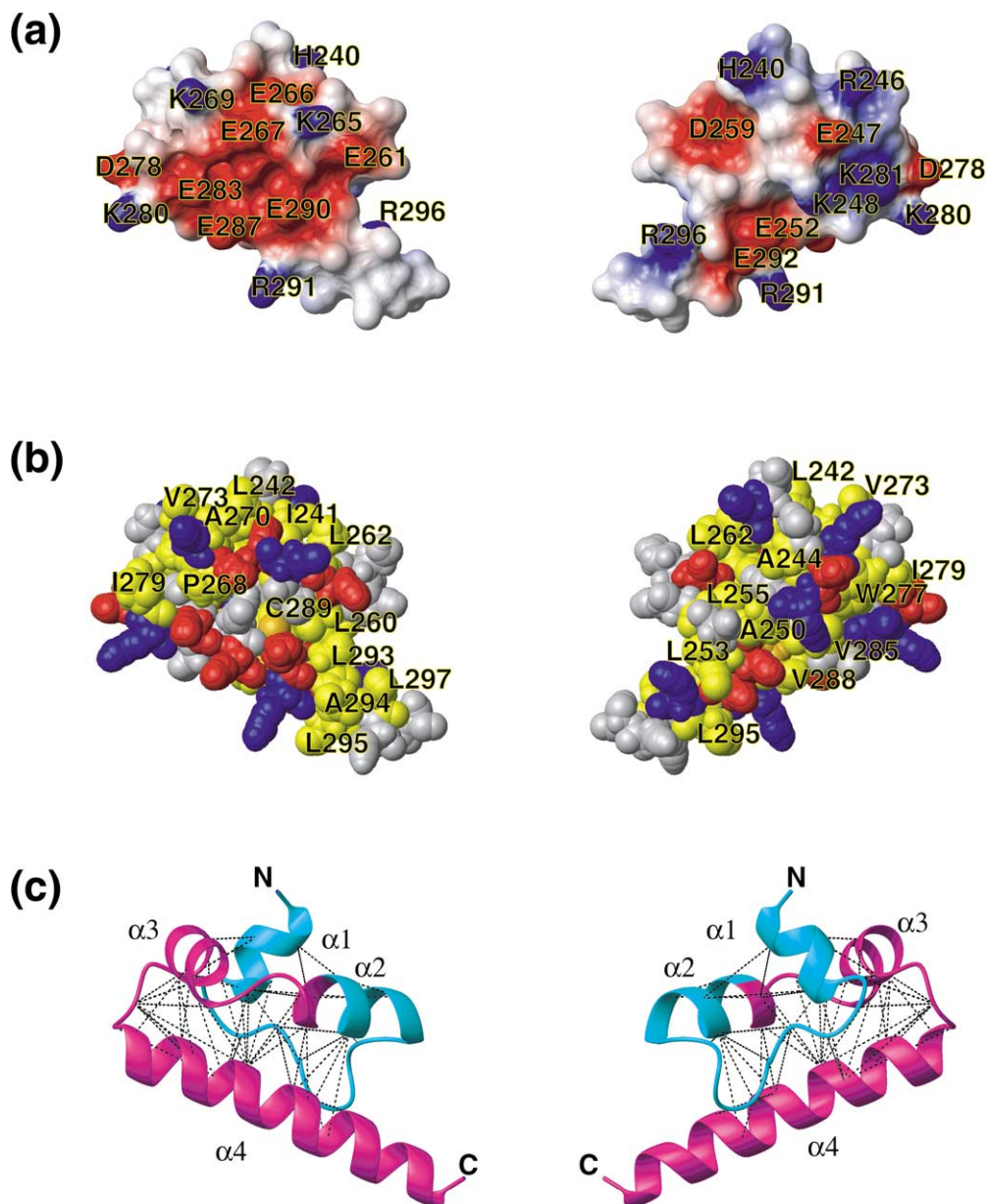


Figure 6. (a) Surface representation of DFF-C (residues 239–300), colored according to the electrostatic potential. Regions with potentials $< -3K_bT$ and $> +3K_bT$ (where K_b is the Boltzman constant and T is the absolute temperature) are represented in red and blue, respectively (calculated with the Delphi module of Insight II; Molecular Simulations Inc). (b) The Van der Waals surface of DFF-C. Atoms belonging to positive residues (R, K, and H) are colored blue, negative residues (E and D) are colored red, and hydrophobic residues (L, V, and I) are colored yellow. C289 is shown in orange. (c) Ribbon model of DFF-C. Residues 239–300 are shown from the same directions. Residues present in both DFF-35 and DFF-45 (239–261) are colored cyan, and those present only in DFF-45 (262–300) are magenta. The broken lines represent long-range NOEs on a residue basis. (b) and (c) were generated with MOLMOL.³⁷

Thus, one can speculate that an involvement of C289 in the chaperone activity would require a dramatic conformational change to expose this cysteine residue to DFF40.

No DFF-C-like structure is present in DREP-1

DREP-1/dICAD is the *Drosophila* homologue of DFF45.^{12,13} It inhibits DNA fragmentation by the DFF40 *Drosophila* homologue, and a significant sequence similarity exists between their N-terminal

regions, indicating that DREP-1 contains a CD domain (37% identity between the CD domains of DREP-1 and mCAD¹³). On the other hand, the putative sequence similarity reported between their C-terminal regions is much less significant, especially near the DFF-C region.^{12,13}

The solution structure of DFF-C does not provide clues that would corroborate previous sequence alignment attempts^{12,13} of the C-terminal sequence of DREP-1 with that of DFF-C. In particular, neither the residues stabilizing the

hydrophobic core nor the charged residues clustering on the molecular surface are conserved. Moreover, the secondary structure prediction correctly predicts that DFF-C is a helical protein, whereas the same prediction program suggests that the C-terminal domain of DREP-1 contains mainly β strands. Thus, although DREP-1 definitely inhibits dCAD and is thus the demonstrated *Drosophila* equivalent of DFF45/ICAD, both the sequence and the structural information presented here strongly suggest that DREP-1 lacks a DFF-C domain.

Conclusion

We determined the first structure of the C-terminal structural domain of DFF45, DFF-C, which is composed of four helices folded in a novel packing arrangement. DFF-C has a large negatively charged patch, suggesting that charge complementation facilitates the interaction of DFF-C with the positively charged C-terminal catalytic domain of DFF40. Based on the structure of DFF-C, the absence of a DFF40-specific chaperone activity for DFF35 can be rationalized by the disruption of the DFF-C structure, particularly of the negatively charged residue cluster. Additionally, our comparison of the DFF45 structure and sequence with the DREP-1 sequence suggests that DREP-1 lacks a structural equivalent of the DFF-C domain.

Materials and Methods

Sample preparation

The DNA sequence encoding residues 225–307 of DFF45 was generated from a HeLa cell cDNA library (Invitrogen) by polymerase chain reaction (PCR) and was ligated to pET15b (Novagen) at the *NdeI/XhoI* sites. Uniformly ^{15}N and ^{15}N , ^{13}C -labeled samples were prepared in M9 medium supplemented with 1 g/l of $^{15}\text{NH}_4\text{Cl}$ and 3 g/l of ^{13}C -labeled D-glucose as the nitrogen and carbon sources, respectively. After expression, the protein was purified by nickel column chromatography. Subsequently, the His tag was cleaved with thrombin and was removed by a second passage through the nickel column. The protein was purified further by reversed phase HPLC, and its identity was confirmed by MALDI-TOF mass spectroscopy (calculated = 9623.9 Da, measured = 9629.34 Da).

Circular dichroism

Measurements were performed with a 1 cm optical path-length cuvette on a JASCO J720 spectrometer equipped with a temperature-control unit. DFF-C was dissolved in 5 mM phosphate buffer (pH 6.5) at a concentration of 10 μM , as determined by the extinction coefficient of the tryptophan residue. The temperature was raised at a rate of 1 $^\circ\text{C}/\text{minute}$.

NMR spectroscopy

The protein concentration was between 700 μM and 3.0 mM, in 20 mM potassium phosphate buffer (pH 6.5), 5 mM DTT. The spectra used for the structure determination were measured at 25 $^\circ\text{C}$ with a protein concentration of 2.0 mM on a Bruker DRX 600 spectrometer. Standard HNCO, HN(CA)CO, HNCA, HN(CO)CA, CBCA(CO)NH, CBCANH, and ^{15}N -edited NOESY-HSQC (mixing time 80 ms) experiments were used for the backbone assignments, and HCCH-total correlation spectroscopy (TOCSY), 3D ^{15}N - and ^{13}C -edited NOESY-HSQC spectra were used for the side-chain assignments.²³ The NOE signals were collected on 3D ^{15}N - and ^{13}C -edited NOESY-HSQC spectra (mixing time 100 ms at 25 $^\circ\text{C}$). NMR spectra were processed using NMRPipe²⁴ and NMRview.²⁵

Residual dipolar couplings

The residual dipolar couplings were determined essentially as described.²⁶ The anisotropic medium we employed was a nematic phase liquid crystalline state induced by Pf1 phage.²⁰ The final optimized Pf1 phage concentration was 20 mg/ml for 1.0 mM DFF-C (see the following section). A 2D-IPAP (^1H - ^{15}N) experiment was used to measure the J_{NH} values.²⁷ A total of 512 complex $f1$ (^{15}N) and 2048 complex $f2$ (^1H) points were recorded with 48 scans per $f1$ increment. The spectral widths were 1460 Hz and 12,020 Hz for $f1$ and $f2$, respectively. The indirect dimension was zero-filled to 2048 points in the final data matrix. A Gaussian apodization window was used to process the $f1$ and $f2$ free induction decays.

Initial estimations for the axial component of the molecular alignment tensor (D_a) and the rhombicity (R) were obtained from the powder pattern distribution of the overall $^1D_{\text{NH}}$ values. These values were then optimized in a stepwise manner, using the calculated solution structure of DFF-C as described.²⁶ The final values of D_a and R for DFF-C were 11.5 Hz and 0.34, respectively.

Relaxation measurements

The ^1H - ^{15}N heteronuclear NOE (hNOE) measurements were performed according to the described method,²⁸ at pH 6.5 and 25 $^\circ\text{C}$, with a proton resonance frequency of 800 MHz. A ^{15}N spin-lock spaced 1.2 ms apart was used in the T_2 experiments to minimize the effects of the resonance offset and of the field inhomogeneity. For the T_2 measurements, eight delay times of 1.6, 3.2, 8.0, 14.4, 24.0, 40.0, 81.6, 161.6, and 241.6 ms were used, with a recycle delay time of 3.0 seconds. In order to quantify the signal intensities, a Lorentzian-to-Gaussian window with a Lorentzian linewidth of 15 Hz and a Gaussian linewidth of 20 Hz was applied in both dimensions, prior to Fourier transformation.²⁹ A fifth-order polynomial baseline correction was subsequently applied in the $f1$ dimension.

Structure calculation

An initial calculation was carried out with all NOE-derived constraints set to 1.8–5.0 \AA , and with the backbone ϕ , ψ torsion angles restrained according to the C^α , C^β and the following residue's CO chemical shifts, using the program TALOS.¹⁹ The calculations were started with extended structures,³⁰ and consisted of a torsion angle space dynamics (TAD), followed by a Cartesian minimization.³¹ The TAD consisted of 10,000

molecular dynamics steps of 15 ps, performed at 50,000 K, and a cooling phase (60,000 steps of 2 fs each) with temperature annealing from 50,000 K to 0 K. A second TAD cooling phase, consisting of 40,000 steps of 1 fs each, was applied with temperature annealing from 1000 K to 0 K. All parameters were scaled to default values.

Ten resultant structures with the lowest overall energies were selected and used as the starting structures for a second calculation to refine the structures. At this stage, the NOE-derived inter-proton distance restraints were classified into three categories: 1.8–3.5 Å, 1.8–4.0 Å, and 1.8–5.0 Å, corresponding to strong, medium and weak NOE intensities, respectively. The hydrogen bond restraints (two per hydrogen bond) were set to $r_{\text{NH-O}} = 1.7\text{--}2.3$ Å and $r_{\text{N-O}} = 2.7\text{--}3.3$ Å, according to the TALOS-based secondary structure identification and the backbone NOE patterns. The residual dipolar coupling derived restraints were used in the SANI modules³² for performing a direct refinement against the measured dipolar couplings with the program CNS version 1.0.³³ The final energy minimization was performed with the following force-field values: 1000 kcal mol⁻¹ Å⁻¹ (1 cal = 4.184 J) for bond lengths, 500 kcal mol⁻¹ rad⁻¹ for angles and improper torsions (which served to maintain planarity and chirality), 4 kcal mol⁻¹ Å⁻¹ for the quartic Van der Waals repulsion term, 50 kcal mol⁻¹ Å⁻¹ for the experimental distance restraints, and 1.0 kcal mol⁻¹ Hz⁻² for the ¹D_{NH} residual dipolar coupling restraints.

²H-exchange

Amide proton exchange rates were measured as described³⁴ at 15 °C by dissolving lyophilized samples buffered at pH 6.5 in ²H₂O. The fractions of unexchanged protons were calculated by the volume integration of peaks in the HSQC spectra measured at 40 minute intervals. The exchange rates of residues S228, A238, and L245, whose amide protons exchanged rapidly, were determined at pH 5.5. The effect of the pH in the exchange rates was corrected when computing the NH-exchange protection factor, which is the ratio between the observed exchange rate and its amino acid intrinsic exchange rate, as reported by Bai *et al.*²² Thus, a protection factor of 100 indicates that this amide proton is protected 100-fold, as compared to the same amino acid in an unstructured polypeptide.

Protein Data Bank accession number

The coordinates are deposited at the RCSB Protein Data Bank under the accession number 1KOY. The chemical shifts are available at the BioMagResBank (BMRB) under accession number 5408.

Acknowledgments

We thank Eiko Matsumoto for plasmid construction, and Makoto Inoue and members of the Protein Research Group for discussion and advice.

References

- Jacobson, M. D., Weil, M. & Raff, M. C. (1997). Programmed cell death in animal development. *Cell*, **88**, 347–354.
- Compton, M. M. (1992). A biochemical hallmark of apoptosis: internucleosomal degradation of the genome. *Cancer Metastasis Rev.* **11**, 105–119.
- Wyllie, A. H., Morris, R. G., Smith, A. L. & Dunlop, D. (1984). Chromatin cleavage in apoptosis: association with condensed chromatin morphology and dependence on macromolecular synthesis. *J. Pathol.* **142**, 67–77.
- Enari, M., Sakahira, H., Yokoyama, H., Okawa, K., Iwamatsu, A. & Nagata, S. (1998). A caspase-activated DNase that degrades DNA during apoptosis, and its inhibitor ICAD. *Nature*, **391**, 43–50.
- Liu, X., Zou, H., Slaughter, C. & Wang, X. (1997). DFF, a heterodimeric protein that functions downstream of caspase-3 to trigger DNA fragmentation during apoptosis. *Cell*, **89**, 175–184.
- Sakahira, H., Enari, M. & Nagata, S. (1998). Cleavage of CAD inhibitor in CAD activation and DNA degradation during apoptosis. *Nature*, **391**(6662), 96–99.
- Zhang, J., Liu, X., Scherer, D. C., van Kaer, L., Wang, X. & Xu, M. (1998). Resistance to DNA fragmentation and chromatin condensation in mice lacking the DNA fragmentation factor 45. *Proc. Natl Acad. Sci. USA*, **95**, 12480–12485.
- Sakahira, H., Iwamatsu, A. & Nagata, S. (2000). Specific chaperone-like activity of inhibitor of caspase-activated DNase for caspase-activated DNase. *J. Biol. Chem.* **275**(11), 8091–8096.
- Otomo, T., Sakahira, H., Uegaki, K., Nagata, S. & Yamazaki, T. (2000). Structure of the heterodimeric complex between CAD domains of CAD and ICAD. *Nature Struct. Biol.* **7**(8), 658–662.
- Zhou, P., Lugovskoy, A. A., McCarty, J. S., Li, P. & Wagner, G. (2001). Solution structure of DFF40 and DFF45 N-terminal domain complex and mutual chaperone activity of DFF40 and DFF45. *Proc. Natl Acad. Sci. USA*, **98**, 6051–6055.
- Inohara, N., Koseki, T., Chen, S., Benedict, M. A. & Nunez, G. (1999). Identification of regulatory and catalytic domains in the apoptosis nuclease DFF40/CAD. *J. Biol. Chem.* **274**, 270–274.
- Inohara, N., Koseki, T., Chen, S., Wu, X. & Nunez, G. (1998). CIDE, a novel family of cell death activators with homology to the 45 kDa subunit of the DNA fragmentation factor. *EMBO J.* **17**, 2526–2533.
- Mukae, N., Yokoyama, H., Yokokura, T., Sakoyama, Y., Sakahira, H. & Nagata, S. (2000). Identification and developmental expression of inhibitor of caspase-activated DNase (ICAD) in *Drosophila melanogaster*. *J. Biol. Chem.* **275**, 21402–21408.
- McCarty, J. S., Toh, S. Y. & Li, P. (1999). Multiple domains of DFF45 bind synergistically to DFF40: roles of caspase cleavage and sequestration of activator domain of DFF40. *Biochem. Biophys. Res. Commun.* **264**, 181–185.
- Gu, J., Dong, R. P., Zhang, C., McLaughlin, D. F., Wu, M. X. & Schlossman, S. F. (1999). Functional interaction of DFF35 and DFF45 with caspase-activated DNA fragmentation nuclease DFF40. *J. Biol. Chem.* **274**, 20759–20762.
- Chen, D., Stetler, R. A., Cao, G., Pei, W., O'Horo, C., Yin, X. M. & Chen, J. (2000). Characterization of the rat DNA fragmentation factor 35/inhibitor of caspase-activated DNase (short form). The endogenous

- inhibitor of caspase-dependent DNA fragmentation in neuronal apoptosis. *J. Biol. Chem.* **275**, 38508–38517.
17. Sakahira, H., Enari, M. & Nagata, S. (1999). Functional differences of two forms of the inhibitor of caspase-activated DNase, ICAD-L, and ICAD-S. *J. Biol. Chem.* **274**, 15740–15744.
 18. Samejima, K. & Earnshaw, W. C. (2000). Differential localization of ICAD-L and ICAD-S in cells due to removal of a C-terminal NLS from ICAD-L by alternative splicing. *Expt. Cell. Res.* **255**, 314–320.
 19. Cornilescu, G., Delaglio, F. & Bax, A. (1999). Protein backbone angle restraints from searching a database for chemical shift and sequence homology. *J. Biomol. NMR*, **13**, 289–302.
 20. Hansen, M. R., Mueller, L. & Pardi, A. (1998). Tunable alignment of macromolecules by filamentous phage yields dipolar coupling interactions. *Nature Struct. Biol.* **5**, 1065–1074.
 21. Holm, L. & Sander, C. (1993). Protein structure comparison by alignment of distance matrices. *J. Mol. Biol.* **233**, 123–138.
 22. Bai, Y., Milne, J. S., Mayne, L. & Englander, S. W. (1993). Primary structure effects on peptide group hydrogen exchange. *Proteins: Struct. Funct. Genet.* **17**, 75–86.
 23. Cavanagh, J., Fairbrother, W., Palmer, A. & Skelton, N. (1996). *Protein NMR Spectroscopy Principle and Practice*. Academic Press, San Diego.
 24. Delaglio, F., Grzesiek, S., Vuister, G. W., Zhu, G., Pfeifer, J. & Bax, A. (1995). NMRPipe: a multidimensional spectral processing system based on UNIX pipes. *J. Biomol. NMR*, **6**, 277–293.
 25. Johnson, B. & Blevins, R. (1994). A computer program for the visualization and analysis of NMR data. *J. Biomol. NMR*, **4**, 603–614.
 26. Kikuchi, J., Iwahara, J., Kigawa, T., Murakami, T., Okazaki, T. & Yokoyama, S. (2002). Solution structure determination of the two DNA-binding domains in the *Shizosaccharomyces pombe* Abp1 protein by a combination of dipolar coupling and diffusion anisotropy restraints. *J. Biomol. NMR*, **22**, 333–347.
 27. Ottiger, M., Delaglio, F. & Bax, A. (1998). Measurement of *J* and dipolar couplings from simplified two-dimensional NMR spectra. *J. Magn. Reson.* **131**, 373–378.
 28. Bax, A. & Grzesiek, S. (1993). Methodological advances in protein NMR. *Acc. Chem. Res.* **26**, 131–138.
 29. Mandel, A. M., Akke, M. & Palmer, A. G., III (1995). Backbone dynamics of *Escherichia coli* ribonuclease HI: correlations with structure and function in an active enzyme. *J. Mol. Biol.* **246**, 144–163.
 30. Nilges, M., Gronenborn, A. M., Brünger, A. T. & Clore, G. M. (1988). Determination of three-dimensional structures of proteins by simulated annealing with interproton distance restraints. Application to crambin, potato carboxypeptidase inhibitor and barley serine proteinase inhibitor 2. *Protein Eng.* **2**, 27–38.
 31. Stein, E. G., Rice, L. M. & Brünger, A. T. (1997). Torsion-angle molecular dynamics as a new efficient tool for NMR structure calculation. *J. Magn. Reson.* **124**, 154–164.
 32. Clore, G. M., Gronenborn, A. M. & Bax, A. (1998). A robust method for determining the magnitude of the fully asymmetric alignment tensor of oriented macromolecules in the absence of structural information. *J. Magn. Reson.* **133**, 216–221.
 33. Brünger, A. T., Adams, P. D., Clore, G. M., DeLano, W. L., Gros, P., Grosse-Kunstleve, R. W. *et al.* (1998). Crystallography and NMR system: a new software suite for macromolecular structure determination. *Acta Crystallog. sect. D*, **54**, 905–921.
 34. Kuroda, Y., Nakai, T. & Ohkubo, T. (1994). Solution structure of a *de novo* helical protein by 2D-NMR spectroscopy. *J. Mol. Biol.* **236**, 862–868.
 35. Kabsch, W. & Sander, C. (1983). Dictionary of protein secondary structure: pattern recognition of hydrogen-bonded and geometrical features. *Biopolymers*, **22**(12), 2577–2637.
 36. Zweckstetter, M. & Bax, A. (2000). Prediction of sterically induced alignment in a dilute liquid crystalline phase: aid to protein structure determination by NMR. *J. Am. Chem. Soc.* **122**, 3791–3792.
 37. Koradi, R., Billeter, M. & Wüthrich, K. (1996). MOLMOL: a program for display and analysis of macromolecular structures. *J. Mol. Graph.* **14**, 51–55.
 38. Laskowski, R. A., Rullmann, J. A., MacArthur, M. W., Kaptein, R. & Thornton, J. M. (1996). AQUA and PROCHECK-NMR: programs for checking the quality of protein structures solved by NMR. *J. Biomol. NMR*, **8**, 477–486.

Edited by M. F. Summers

(Received 5 April 2002; received in revised form 5 June 2002; accepted 5 June 2002)